# Coulomb and nuclear breakup of <sup>8</sup>B

## R. Shyam

Saha Institute of Nuclear Physics, Calcutta - 700 064, India E-mail address: shyam@tnp.saha.ernet.in

### I.J. Thompson

Department of Physics, University of Surrey, Guildford GU2 5XH, U.K. E-mail address: I.Thompson@surrey.ac.uk (September 24, 2018)

## Abstract

The cross sections for the (<sup>8</sup>B, <sup>7</sup>Be-p) breakup reaction on <sup>58</sup>Ni and <sup>208</sup>Pb targets at the beam energies of 25.8 MeV and 415 MeV have been calculated within a one-step prior-form distorted-wave Born approximation. The relative contributions of Coulomb and nuclear breakup of dipole and quadrupole multipolarities as well as their interference have been determined. The nuclear breakup contributions are found to be substantial in the angular distributions of the <sup>7</sup>Be fragment for angles in the range of 30° - 80° at 25.8 MeV beam energy. The Coulomb-nuclear interference terms make the dipole cross section larger than that of quadrupole even at this low beam energy. However, at the incident energy of 415 MeV, these effects are almost negligible in the angular distributions of the (<sup>7</sup>Be-p) coincidence cross sections at angles below 4°.

PACS NO. 25.70.De, 25.40.Lw, 96.60.Kx

KEYWORDS: Coulomb and nuclear breakup of  $^8$ B, prior-form DWBA theory, E1 and E2 breakup cross sections, nuclear breakup effects.

### I. INTRODUCTION

The Coulomb dissociation (CD) method provides an alternate indirect way to determine the cross sections for the radiative capture reaction  $^7\text{Be}(p,\gamma)^8\text{B}$  at low relative energies [1,2], which is the most important and most uncertain nuclear input to the standard solar model calculations [3,4]. The CD method reverses the radiative capture by the dissociation of a projectile (the fused system) in the Coulomb field of a target by making the assumption that nuclei do not interact strongly and the electromagnetic excitation process is dominated by a single multipolarity.

Motobayashi et al. performed the first measurement of the breakup of  $^8B$  into  $^7Be-p$  low energy continuum in the field of  $^{208}Pb$  with a radioactive  $^8B$  beam of 46.5 MeV/A energy [5], which was analyzed by us [6] using Alder-Winther's semiclassical theory of Coulomb excitation (which assumes the colliding nuclei are point-like objects) [7]. Considering only the E1 component of the excitation, we found [6] the measured breakup cross sections to be consistent with a  $S_{17}(0) = (15.5 \pm 2.80)$  eV barn. However, in the CD of  $^8B$  at these energies, the E2 component of breakup may not be negligible [8], and its presence affects the extracted  $S_{17}(0)$  [6]. Although some authors [9] dispute this claim, a reliable estimate of this component is necessary for the accurate extraction of the astrophysical S-factor  $(S_{17}(0))$  from the breakup data.

Since the contribution of the E2 component is strongly dependent on the nuclear structure model of  $^8B$  (which is not yet known with certainty), the RIKEN group has repeated the breakup measurements with angular distributions extended to larger scattering angles where the cross sections are more sensitive to the E2 component [10]. An analysis of this data within the distorted wave Born-approximation (where the breakup is treated as the inelastic excitation of the projectile to the continuum) led these authors to conclude that the E2 components and the nuclear breakup effects are considerably smaller. However, they use a collective model prescription to calculate the inelastic nuclear form factor (see eg. [6]). Due to a long tail in the  $^8B$  g.s wave function this procedure is unlikely to be accurate. Furthermore, Coulomb breakup is calculated by a point-like projectile approximation (PLPA) in these studies, and its range of validity is yet to be determined for this projectile.

The Notre Dame group has measured the breakup of <sup>8</sup>B on the <sup>58</sup>Ni target at the beam energy of 25.8 MeV, well below the Coulomb barrier, where the *E*2 component is expected to dominate the CD process [11]. However, the reliable extraction of the *E*2 component from this data, where only the the integrated cross section of the <sup>7</sup>Be fragment is measured, is still doubtful. The analysis of the data reported in Ref. [11] used the Alder-Winter's semiclassical theory of Coulomb excitation, where the final state is treated as a two-body system, thus assuming that the measured angles of <sup>7</sup>Be were equal to those of the <sup>7</sup>Be-*p* center of mass. The inadequacy of this assumption has been demonstrated in [12]. Furthermore, the total breakup cross section reported in this experiment could not be reproduced within the Alder-Winther theory even if a wide variety of structure models of <sup>8</sup>B were used [13]. On the other hand, the importance of the nuclear breakup effects in the kinematical regime of this experiment has recently been emphasized [14]. Therefore, there is a need to reanalyze this data using a proper theory where the three-body kinematics is taken into account.

In this paper we perform a one-step prior-form DWBA analysis of the <sup>8</sup>B breakup data at both low and high energies in order to check the validity of various assumptions of

the Coulomb dissociation method. We describe the breakup process as a single proton excitation of the projectile from its ground state to a range of states in the continuum, which is discretized by the method of continuum bins.

In previous calculations [13,14] based on this model, quadrupole transitions from the ground state to the continuum did not include the excitation of f partial waves in all cases. Moreover, the numerical calculations were performed only for the breakup reaction  $^8B + ^{58}Ni \rightarrow ^7Be + X$  at the beam energy of 25.8 MeV where the final state was considered as as a two-body system. In this work we improve upon this aspect by using a proper three-body kinematics for the final state, and also include excitations of  $\ell = 3$  continuum states everywhere.

We furthermore apply our model to the RIKEN data where  ${}^{7}\text{Be}$  and p were detected in coincidence with very small relative energies in a  ${}^{8}\text{B}$  induced reaction on  ${}^{208}\text{Pb}$  target at the beam energy of 415 MeV. We avoid the point-like projectile approximation as well as collective model prescription for the nuclear form factor, by determining the nuclear and Coulomb parts by a single-folding method where the relevant fragment-target interactions are folded by the projectile wave functions in the ground and continuum states.

We indicate our formalism in the next sections. Details of the numerical calculations are described in section III. The results of our calculations and their discussions are presented in section IV, while the summary and conclusions of our work are given in section V.

### II. FORMALISM

### A. DWBA reaction mechanism

The cross section for the breakup of a projectile (a) into its fragments (c and p),  $t+a \rightarrow c+p+t$ , can be represented to first order by the inelastic excitation of the projectile a to its continuum,  $t+a \rightarrow a^* + t$  by means of the 'prior form' DWBA matrix element. This is an integral of the form

$$T_{DWBA}^{(-)} = \langle \phi_{\mathbf{k}_{cp}}(\mathbf{r}) \chi_{a^*t}^{(-)}(\mathbf{p}_{a^*}, \mathbf{R}) \mid V_{ct}(\mathbf{r}_c) + V_{pt}(\mathbf{r}_p) \mid \phi_0(\mathbf{r}) \chi_{at}^{(+)}(\mathbf{p}_a, \mathbf{R}) \rangle.$$
(1)

In this expression  $\phi_0$  is the ground state wave function of the projectile,  $\chi_{at}^{(+)}(\mathbf{p}_a, \mathbf{R})$  describes the relative motion of the projectile with respect to the target, and  $\phi_{k_{cp}}(\mathbf{r})\chi_{a^*t}^{(-)}(\mathbf{p}_{a^*}, \mathbf{R})$  describes the excited continuum state  $\mathbf{k}_{cp}$  of the projectile fragments after breakup. The superscripts (+) and (-) specify the outgoing or incoming wave boundary conditions satisfied by the corresponding wave functions respectively. The coordinates  $\mathbf{R}$  and  $\mathbf{r}$  describing the motion of the CM of the fragments with respect to the target and their relative motion respectively are related to those of the relative motion of the individual fragments from the target  $(\mathbf{r}_p$  and  $\mathbf{r}_c)$  by

$$\mathbf{r}_{p} = \mathbf{R} + \frac{m_{c}}{m_{a}}\mathbf{r},$$

$$\mathbf{r}_{c} = \mathbf{R} - \frac{m_{p}}{m_{a}}\mathbf{r}.$$
(2)

The  $V_{ct}(\mathbf{r}_c)$  and  $V_{pt}(\mathbf{r}_p)$  are the core (<sup>7</sup>Be) and proton optical potentials, respectively, for interaction with the target.

Alternatively, the DWBA may be regarded as the first iteration of a perturbative solution of a coupled-channels problem, and the breakup cross sections found from the S-matrix elements of the outgoing channels when a set of coupled equations is iterated once. The double differential cross section for a c-p breakup state from ground state spin  $j_a$  into final spin state  $j_{a^*}$  and relative momentum  $k_{cp}$  is given by

$$\frac{d^2\sigma_{\ell}(k_{cp})}{dk_{cp}d\Omega_{a^*}} = \frac{1}{(2j_a+1)} \sum_{m'm} |\sum_{LL'J} \langle L0 \ j_a m | Jm \rangle \langle L'm - m' \ j_{a^*} m' | Jm \rangle 
\times \frac{4\pi}{p_a} \sqrt{\frac{p_{a^*}}{p_a}} e^{i(\sigma_L + \sigma'_{L'})} \frac{i}{2} S^J_{Lj_a, L'j_{a^*}k_{cp}} Y^0_L(0,0) Y^{m-m'}_{L'}(\Omega_{a^*})|^2,$$
(3)

where  $p_a$  is the incident momentum of a in the  $\mathbf{z}$  direction and  $\Omega_{a^*}$  is the direction of momentum  $\mathbf{p_{a^*}}$  of the CM of the c-p system with respect to the target nucleus t. In Eq. (3), J denotes the total angular momentum of the system and L, L' are the initial and final angular momentum of the CM of c-p pair with respect to the target. In this work the S-matrix method has been used, and the following paper [15] continues this approach to present solutions of the full coupled equations, though only at the lower (Notre Dame) sub-Coulomb energy.

Since our approach is based on a first-order solution of the coupled-channels equations, we refer to the accompanying paper [15] (section II), for details of these equations and of the coupling matrix elements. The DWBA results presented below arise from the solution of Eq.(5) of [15] for n = 1. This implies that the entrance and exit channel potentials for the  $\chi_{at}^{(+)}(\mathbf{K}_i, \mathbf{R})$  and  $\chi_{a^*t}^{(-)}(\mathbf{K}_f, \mathbf{R})$  channel wave functions are not optical potentials, but are the diagonal interactions found by folding the fragment potentials  $V_{ct}(\mathbf{r}_c) + V_{pt}(\mathbf{r}_p)$  over the initial or final states. These states are either the initial state  $\phi_0$  or the continuum bin states ( [15], Eq. 6) for the bin centers and widths to be described below.

### B. Coincidence cross sections

The *triple* differential cross section for the breakup of a projectile a into its fragments c and p can be related to the *double* differential cross sections shown in [15] (for the inelastic excitation of the projectile a to its continuum state  $\mathbf{k}_{cp}$ ). This is accomplished, as in [12], by

$$\frac{d^3\sigma}{dE_c d\Omega_c d\Omega_p} = \frac{J'}{4\pi} \frac{d^2\sigma}{dE_{cp} d\Omega_{a^*}} \frac{\partial E_p}{\partial E_{tot}},\tag{4}$$

where the total kinetic energy

$$E_{tot} = E_c + E_p + E_t$$
  
=  $E_{cp} + E_{a^*} + \frac{P^2}{2(m_a + m_t)}$ . (5)

is related to the projectile energy  $(E_a)$  and the reaction Q-value (Q) by  $E_{tot} = E_a + Q$ . In Eq. (5)  $E_c$ ,  $E_p$ , and  $E_t$  are the kinetic energies of the fragments c, p and recoiling target nucleus respectively, while  $E_{cp}$  and  $E_{a^*}$  are the kinetic energies of the relative motion of

the fragments and of their CM with respect to the target nucleus respectively. In Eq. (4), we have assumed that the angular distribution of fragments is isotropic in the projectile rest frame; the expressions without making this assumption are given in Ref. [16]. The last factor in Eq. (4) is given by

$$\frac{\partial E_p}{\partial E_{tot}} = m_t \left[ m_p + m_t - m_p \frac{\mathbf{p}_p \cdot (\mathbf{P} - \mathbf{p}_c)}{p_p^2} \right]^{-1}, \tag{6}$$

and the Jacobian J' is defined as

$$J' = \frac{m_c p_c m_p p_p}{\mu_{cp} p_{cp} \mu_{at} p_{a^*}} . \tag{7}$$

In Eqs. (2, 6, 7),  $m_i$  is the mass of the fragment i, and  $\mu_{at}$  and  $\mu_{cp}$  are the reduced masses of the a-t and c-p systems respectively.  $\mathbf{P}$  is the total momentum which is fixed by the conditions in the entrance channel. The momenta  $\mathbf{p}_{cp}$  and  $\mathbf{p}_{a^*}$ , describing the relative motion of the fragments c and p and the motion of their CM with respect to the target nucleus respectively, can be related to their individual momenta  $\mathbf{p}_c$  and  $\mathbf{p}_p$  by straightforward expressions (see. e.g. Ref. [17,12]).

## III. THE NUMERICAL PROCEDURE AND APPLICATION TO <sup>8</sup>B BREAKUP

The <sup>8</sup>B nucleus has a 2<sup>+</sup> ground state at -0.137 MeV, which is composed predominantly of the <sup>7</sup>Be core in its  $3/2^-$  ground state and a valence proton in a  $p_{3/2}$  configuration. E1 ( $\lambda=1$ ) and E2 ( $\lambda=2$ ) mechanisms will populate the ( $s_{1/2}$ ,  $d_{3/2}$ ,  $d_{5/2}$ ) and ( $p_{1/2}$ ,  $p_{3/2}$ ,  $f_{5/2}$ ,  $f_{7/2}$ ) single particle continuum states respectively in the first step. We consider the excitation to states of these partial waves up to  $E_{p-7Be}=3$  MeV.

We have taken a single particle model for the structure of <sup>8</sup>B assuming that all states in <sup>8</sup>B are determined by the g.s. potential defined in [21]. This simplification of the <sup>7</sup>Be-*p* scattering state interaction, neglecting the core couplings and the M1 transitions, has hardly any effect on the integrated CD cross section ([13]) at non-relativistic energies.

As remarked earlier, in the DWBA calculations we have to use diagonal channel potentials for the entrance and exit channels. Different choices for these potentials are (a) pure  $^8B$ +target Coulomb, (b) Coulomb + some fixed optical potential, or (c) using the monopole ( $\lambda=0$ ) parts of the single-folded potentials (eq. (15) of [15]). Choice (a) is appropriate for comparison with simple (e.g. semiclassical) models. Choice (b) is inaccurate for breakup states, as can be seen by comparison with the very diffuse potentials found in method (c). Choice (c) has the advantage that it generalizes readily when all the diagonal/off-diagonal monopole/multipole couplings need to be calculated for a full CDCC calculation as in [15].

For the Notre Dame experiment on the Coulomb dissociation of  $^8\mathrm{B}$  on  $^{58}\mathrm{Ni}$  at 26 MeV [11], good accuracy for the continuum discretization is obtained if we use 13 bins per partial wave, defined in the following way: 9 bins of 100 keV centered at 0.15; 0.25; ...; 0.95 MeV and 4 bins of 500 keV centered at 1.25; 1.75; 2.25; 2.75 MeV. Sufficient convergence for the E1 and E2 transitions was obtained if the maximum number of the partial waves ( $l_{max}$ ) and the maximum radius ( $R_{max}$ ) were taken to be  $600\hbar$  and 300 fm respectively. Coupled asymptotic wave functions [24] are used beyond 30 fm.

For the RIKEN experiment on the Coulomb dissociation of <sup>8</sup>B on <sup>208</sup>Pb at 415 MeV [10], good accuracy for the continuum discretization is obtained if we use 8 bins per partial wave, defined in the following way: 4 bins of 250 keV centered at 0.125; 0.375; 0.625; 0.875 MeV and 4 bins of 500 keV centered at 1.25; 1.75; 2.25; 2.75 MeV. The bin wave functions were each integrated with 200 k-steps, out to  $R_m = 50$  fm. In order to obtain convergence for the E1 and E2 transitions in this case, we include up to  $l_{max} = 10000\hbar$  and  $R_{max} = 1000$  fm for the reaction mechanism. Coupled asymptotic wave functions [24] are used beyond 50 fm.

### IV. RESULTS AND DISCUSSION

In Figs. 1a and 1b, we show the angular distributions of  $^7\mathrm{Be}$  and  $^8\mathrm{B}^*$  respectively in a  $^8\mathrm{B}$  induced breakup reaction on  $^{58}\mathrm{Ni}$  target at the beam energy of 25.8 MeV. Pure Coulomb and pure nuclear breakup cross sections are represented by the dashed and dashed-dotted curves respectively. The cross sections obtained by summing coherently the Coulomb and nuclear amplitudes (to be referred as total in the following) are represented by the solid lines. In these calculations the procedure of single-folding the respective fragment-target interactions with  $^8\mathrm{B}$  ground and continuum state wave functions (Eq. (11)) have been used. Nuclear parts of  $p^{-58}\mathrm{Ni}$  and  $^7\mathrm{Be}^{-58}\mathrm{Ni}$  interactions have been taken from Refs. [25] and [26] respectively. The curves in Fig. 1b improve on those in [14] by the inclusion of f-wave final states.

The angular distributions of  ${}^{7}\text{Be}$  and  ${}^{8}\text{B}^{*}$  are distinctly different from each other. While pure Coulomb and total breakup cross sections show a forward peak in case of  ${}^{7}\text{Be}$  (which is typical of the angular distribution of fragments emitted in breakup reactions), those of  ${}^{8}\text{B}^{*}$  tend to zero as angle goes to zero. The latter is the manifestation of the adiabatic cut-off typical of the Coulomb-excitation process. In both the cases the nuclear effects are small below  $20^{\circ}$  and there is a Coulomb-nuclear interference minimum between  $25^{\circ}$  -  $60^{\circ}$ . However the magnitude of various cross sections are smaller in Fig. 1a. Furthermore, the nuclear-dominated peak occurs at different angles in Figs 1a ( $\simeq 55^{\circ}$ ) and 1b ( $\simeq 70^{\circ}$ ). As discussed in section (2.1), the angles of  ${}^{7}\text{Be}$  can be related to those of  ${}^{8}\text{B}^{*}$ . A given  $\theta_{7_{Be}}$  gets contributions from a range of generally larger  $\theta_{8_{B^{*}}}$ . This explains to some extent the shifting of the peaks of various curves to lower angles in Fig. 1a as compared to the corresponding ones in Fig. 1b. This underlines the important of three-body kinematics in describing the inclusive breakup reactions.

The ratio of the experimental integrated breakup cross section of  $^7$ Be (obtained by integrating the breakup yields in the angular range,  $(45 \pm 6)^{\circ}$ , of the experimental setup) to Rutherford elastic scattering of  $^8$ B is reported to be  $(8.1 \pm 0.8^{+2.0}_{-0.5}) \times 10^{-3}$  [11]. It is not possible to get this cross section by directly integrating the angular distributions shown in Fig. 1b in this angular range as the corresponding angles belong to  $^8$ B\* and not to  $^7$ Be. However, in the three-body case (Fig. 1a), this can be done in a straight-forward way. This gives a value of  $7.0 \times 10^{-3}$  which is in close agreement with the experimental data. Thus, previous failures to explain the experimental value may be attributed to the neglect of both the Coulomb-nuclear interference effects and the three-body kinematics.

In Fig. 2, we have investigated the range of the validity of the point-like projectile approximation (PLPA) and the role of the Coulomb-nuclear interference effects on the cross sections of dipole and quadrupole components for the reaction discussed in Fig. 1a. In Fig.

2a the results for pure Coulomb breakup are shown. Dipole and quadrupole components of the cross section obtained by the single-folding procedure are shown by solid and dashed lines respectively, while those obtained with the PLPA by solid and dashed lines with solid circles. It can be noted that PLPA is not valid for angles beyond  $20^{\circ}$ . The condition that the impact parameter of the collision is larger than the sum of the projectile and target radii ( $b > R_a + R_t$ ), assumed in applying the Alder-Winther theory, is no longer valid because there is a long tail in the <sup>8</sup>B ground state wave function. We also note that the quadrupole component is affected more by the PLPA as compared to the dipole. The big difference in the dipole and quadrupole cross sections seen in the PLPA results beyond  $20^{\circ}$  (where the quadrupole component is much bigger than the dipole), almost disappears in the corresponding cross sections obtained by single-folding procedure. Nevertheless, the quadrupole cross sections still remain larger than those of the dipole beyond  $30^{\circ}$  in the latter case.

In connection with PLPA, it should be made clear that p + target and the <sup>7</sup>Be + target potentials do take into account the finite size of the <sup>7</sup>Be and target nuclei. This effect, however, is only important when two nuclei are very close to each other and is masked by the nuclear effects which would be important at those impact parameters.

Dipole and quadrupole cross sections for pure nuclear breakup are shown in Fig. 2b. The cross sections obtained by summing coherently the amplitudes of E1 and E2 components of pure Coulomb and pure nuclear breakup are shown in Fig. 2c. We shall still refer the corresponding components of the total cross sections as E1 and E2, although usually the dipole and quadrupole components of the pure Coulomb cross sections are referred as such. We notice that the Coulomb-nuclear interference effects make the contributions of the dipole component of the total cross section larger than those of quadrupole one at all the angles. This result is quite remarkable as it implies that the E2 component of the total break up cross section in the  $^8B$  induced reaction on  $^{58}N$ i target is not dominant even at the subCoulomb beam energies. Therefore, there is hardly any hope of determining the E2 component of  $^8B$  breakup by Notre Dame type of experiment [11].

This underlines the need for more refined experiments to determine the E2 component (as already pointed out in Ref. [8]). It is clear from Fig. 2c that the measurements of the angular distributions may provide useful information about the E2 component as it is different from that of the E1 multipolarity. On the other hand, the angular distributions of the fragments, calculated within a semiclassical theory without making the approximation of isotropic angular distributions in the projectile rest frame, have been shown to have large E1 - E2 interference effects [28,29]. They lead to asymmetries in the momentum distributions of the fragments, whose measurements may enable one to put constraints on the E2 component [30]. However, for the better accuracy of this method, improved calculations including the nuclear effects may be necessary.

Our results for the nuclear effects in the angular distribution of <sup>8</sup>B\* are approximately similar to that reported in [31], where Coulomb and nuclear form factors are calculated by folding the proton-target mean-field (parameterized by a Woods-Saxon function) by the ground and discretized continuum state <sup>8</sup>B wave functions. These authors calculate various cross sections by integrating a fixed projectile-target optical potential along a semiclassical trajectory. However, since the three-body kinematics for the final state has not been considered by them, a direct comparison between their calculations and the data of [11] is not

possible.

In Fig. 3a, we show E1 and E2 components of the angular distributions for the  $^8\mathrm{B}$  +  $^{208}\mathrm{Pb} \to ^8\mathrm{B}^*$  +  $^{208}\mathrm{Pb}$  reaction measured by the Kikuchi et al. [10] at the beam energy of 415 MeV, for the pure Coulomb excitation case. The dashed, dotted and solid lines represent E1, E2 and E1 + E2 cross sections respectively which are obtained by the single-folding procedure. Also shown in this figure are the corresponding results obtained by PLPA (curves with solid circles). We note that PLPA becomes inaccurate beyond 4° in this case. Moreover, the E2 component of the pure Coulomb excitation becomes increasingly important also after this angle.

In Fig. 3b, the total cross sections are shown. The nuclear part of the fragment-target interaction at these energies have been taken from [25] (for proton) and [27] (for  $^7$ Be). The dashed and dotted lines show the dipole and quadrupole cross sections respectively, while the solid line represents their sum. It can be noted that nuclear effects modify the pure Coulomb E1 cross sections substantially after  $\sim 4^{\circ}$ , and the E2 cross sections in the entire angular range. However, since the E2 components are quite small at angles  $\leq 4^{\circ}$ , the difference between pure Coulomb and total dipole + quadrupole cross sections is appreciable only after this angle.

Therefore, at RIKEN energies, the PLPA breaks down beyond 4°, where the Coulombnuclear interference effects as well as the quadrupole component of breakup is substantial. Hence, the Coulomb dissociation method as used in e.g. Ref. [6] to extract a reliable  $S_{17}(0)$ from the measurements of the angular distributions in the breakup of <sup>8</sup>B on heavy target at RIKEN energies ( $\sim 50 \text{ MeV/nucleon}$ ), is useful only when data is taken at angles below 4°.

In Figs. 4a, 4b and 4c we show the comparison of our calculations for  $\epsilon \cdot d\sigma/d\theta$  with the experimental data of Kikuchi et al. [10] as a function of the scattering angle  $\theta_{8_{B^*}}$  of the excited  ${}^8B$  (center of mass of the  ${}^7Be+p$  system) for three relative energy bins. We have used the efficiency ( $\epsilon$ ) matrix as well as angular and energy averaging as discussed in Ref. [10] which is provided to us by the RIKEN collaboration. The dashed and dotted lines are the pure Coulomb E1+E2 and E2 cross sections respectively while the solid and dashed lines are the corresponding total cross sections. We note that our calculations are in fair agreement with the experimental data. We stress that no arbitrary normalization constant has been used in the results reported in this figure.

The quadrupole component of breakup is significant at almost all the angles in the relative energy bin 2.0 - 2.25 MeV(c), and at angles beyond 5° in the energy bin 1.25 - 1.50 MeV(b). On the other hand, its contribution is inconsequential in the energy bin 0.5 - 0.75 MeV(a). This result is in somewhat disagreement with that reported in Ref. [10], where this component is reported to be small everywhere below 1.75 MeV relative energy. Although these authors also perform a quantum mechanical calculation within DWBA, their treatment of the continuum state is very different from ours. Moreover they use a collective model prescription for the Coulomb and nuclear form factors, which has a limited applicability for  $^8B$  breakup. Bertulani and Gai [32] have also reported smaller quadrupole component in their analysis of this data. These authors do not include the nuclear effects in the E1 excitations and make use of the eikonal approximation to calculate the quadrupole nuclear excitation amplitudes. Moreover, the Coulomb excitation amplitudes have been calculated with the PLPA which we have found to be invalid at higher angles (see Fig. 3). It is also noted in Fig.3 that Coulomb-nuclear interference effects reduce the E1 cross sections at

larger angles.

Some authors have studied the importance of the higher order effects in the Coulomb breakup of <sup>8</sup>B [33,34,29,35]. At RIKEN energies these effects play only a minor role for this reaction in the kinematical regime of forward angles and low relative energies [33,29,35]. Therefore, our conclusions about the RIKEN data are unlikely to be affected much by the higher order breakup effects. However, the multi-step breakup could play an important role at Notre Dame energies, which is discussed in the following article [15].

Finally we would like to remark that since we have adopted the single particle model of Ref. [29] for the structure of  $^8B$  in our dynamical nuclear reaction calculations, the astrophysical S-factor for the radiative capture reaction  $^7Be(p,\gamma)^8B$  resulting from our analysis of the RIKEN data is the same as that of these authors (17 eV.barn). It is should be noted that unlike the pure Coulomb dissociation calculations this is not a fitting parameter in our analysis.

#### V. SUMMARY AND CONCLUSIONS

In this paper, we studied the breakup reactions  $^8\mathrm{B} + ^{58}\mathrm{Ni} \rightarrow ^7\mathrm{Be} + \mathrm{X}$  and  $^8\mathrm{B} + ^{208}\mathrm{Pb}$   $\rightarrow$   $^8\mathrm{B}^* + ^{208}\mathrm{Pb}$ , at beam energies of 25.8 and 415 MeV respectively, within the framework of the one-step prior-form distorted wave Born-approximation. In this theory, the breakup process is described as a single proton excitation of the projectile from its ground state to a range of states in the continuum, which is discretized by the method of continuum bins. In this method, both Coulomb and nuclear breakup as well as their interference terms are calculated within the same framework. Moreover, we use the three-body kinematics while calculating the cross sections for the  $^7\mathrm{Be}$  fragment in the first reaction.

For the breakup reaction at low energy the Coulomb-nuclear interference effects are found to be quite important. This leads to a reduction in the pure Coulomb dissociation cross sections for the <sup>7</sup>Be fragment in the angular range of the measurements reported in [11], which together with the three-body kinematics reproduces the experimental integrated cross section for this fragment. This agreement had eluded the pure Coulomb dissociation calculations.

A very striking feature of the Coulomb-nuclear interference effect is that it makes the E1 component of the total cross section of the breakup reaction  $^8\mathrm{B} + ^{58}\mathrm{Ni} \to ^7\mathrm{Be} + \mathrm{X}$  (at the beam energy of 25.8 MeV), larger than the corresponding E2 component at all the angles. This renders untenable the main objective of the Notre Dame experiment of determining the E2 component in the breakup of  $^8\mathrm{B}$  at low beam energies. The dominance of the E2 component for this reaction at this energy, seen in the semi-classical Alder-Winther theory of Coulomb excitation has led to this expectation. However, we note that even in pure Coulomb dissociation process, with finite size of the projectile taken into account, the E2 components is almost equal to that of E1 in the relevant angular range.

The breakup data at higher beam energies (RIKEN energies), are almost free from the nuclear effects and are dominated by the E1 component for  $^7\text{Be-}p$  relative energies < 0.75 MeV at very forward angles ( $\le 4^\circ$ ). The study of the breakup of  $^8\text{B}$  in this kinematical regime is, therefore, better suited for the extraction of reliable  $S_{17}(0)$  for the capture reaction  $^7\text{Be}(p,\gamma)^8\text{B}$  at low relative energies.

## ACKNOWLEDGMENTS

One of the authors (RS) would like to acknowledge an associateship award from the Abdus Salam International Centre of Theoretical Physics, Trieste. This work is supported by Engineering and Physical Sciences Research Council, UK, grant nos. J/95867 and L/94574.

## REFERENCES

- [1] G. Baur and H. Rebel, J.Phys.G:Nucl. and Part. Phys. 20, 1 (1994)
- [2] G. Baur and H. Rebel, Ann. Rev. Nuc. Part. Sc. 46, 321 (1997).
- [3] J.N. Bahcall, Neutrino Astrophysics, Cambridge University Press, New York, 1989: J.N. Bahcall, M.H. Pinsonneault, Rev. Mod. Phys. 67, 781 (1995); J.N. Bahcall, Nucl. Phys.A 631, 29 (1998).
- [4] S. Turck-Chieze et al., Phys. Rep. **230**, 57 (1993).
- [5] T. Motobayashi et al., Phys. Rev. Letts. 73, 2680 (1994).
- [6] R. Shyam, I.J. Thompson and A.K. Dutt-Majumder, Phys. Lett.B 371,1 (1996).
- [7] K. Alder and A. Winther, *Electromagnetic Excitation*, (North Holland, Amsterdam, 1975).
- [8] K. Langanke, T.D. Shoppa, Phys. Rev.C **49**, R1771 (1994); **51** (1995) 2844(E); **52** (1995) 1709.
- [9] M. Gai and C.A. Bertulani, Phys. Rev.C **52**, 1706 (1995).
- [10] T. Kikuchi et al., Phys. Letts. **B391**, 261 (1997).
- [11] Johannes von Schwarzenberg et al., Phys. Rev. C53, R2598 (1996).
- [12] R. Shyam and I.J. Thompson, Phys. Lett.B **415**, 315 (1997).
- [13] F.M. Nunes, R. Shyam and I.J. Thompson, J.Phys.G 24, 1575 (1998).
- [14] F.M. Nunes and I.J. Thompson, Phys. Rev.C 57, R2818(1998)
- [15] F.M. Nunes and I.J. Thompson, Phys. Rev. C, following paper.
- [16] G. Baur and M. Weber, Nucl. Phys. A 504, 352 (1989); H. Esbensen and G. Bertsch, Phys. Lett.B 359, 13 (1995).
- [17] H. Fuchs, Nucl. Instr. & Methods 200, 361 (1982); C.A. Bertulani, Phys. Rev. C 49, 2688 (1994).
- [18] G.H. Rawitscher, Phys. Rev. C9, 2210 (1974), C11, 1152 (1975), Nucl. Phys. A241, 365 (1975); M. Yahiro and M. Kamimura, Prog. Theor. Phys. 65, 2046 (1981), 65, 2051 (1981).
- [19] Y. Sakuragi, M. Yahiro and M. Kamimura, Prog. Theor. Phys. Suppl. 89, 136 (1986).
- [20] K.H. Kim, M.H. Park and B.T. Kim, Phys. Rev. C 53, 363 (1987).
- [21] H. Esbensen and G. Bertsch, Nucl. Phys. A 600, 37 (1996).
- [22] Y. Hirabayashi and Y. Sakuragi, Phys. Rev. Lett. **69**, 1892 (1992).
- [23] I.J. Thompson, Computer Physics Reports, 7, 167 (1988).
- [24] J. Christley and I.J. Thompson, Comp. Phys. Comm., 79, 143 (1994).
- [25] F.D. Becchetti and G.W. Greenlees, Phys. Rev. **182**, 1190 (1969).
- [26] C.W. Glover, R.I. Cutler and K.W. Kemper, Nucl. Phys.A **341**, 137 (1980).
- [27] A.F. Zeller, D.C. Weisser, T.R. Ophel and D.F. Hebbard, Nucl. Phys. A 332, 515 (1979).
- [28] H. Esbensen and G.F. Bertsch, Phys. Lett.B **359**, 13(1995).
- [29] H. Esbensen and G.F. Bertsch, Nucl. Phys.A 600, 66 (1996)
- [30] B. Davids et al., Phys. Rev. Lett. **81**, 2209 (1998)
- [31] C.H. Dasso, S.M. Lenzi and A. Vitturi, Nucl. Phys. A. (in press)
- [32] C.A. Bertulani and M. Gai, Nucl. Phys. A **636**, 227 (1998).
- [33] S. Typel and G. Baur, Phys. Rev.C **50**, 2104 (1994).
- [34] H. Esbensen, G.F. Bertsch and C.A. Bertulani, Nucl. Phys. A **581**, 107 (1995).
- [35] S. Typel, H. Wolter and G. Baur, Nucl. Phys.A 617, 147 (1997).

## Figure Captions

- Fig. 1 Angular distribution of the <sup>7</sup>Be fragment emitted in the breakup reaction of <sup>8</sup>B on <sup>58</sup>Ni target at the beam energy of 25.8 MeV. The dashed and dashed-dotted lines show the pure Coulomb and pure nuclear breakup cross sections respectively while their coherent some is represented by the solid line. (b) Angular distribution of <sup>8</sup>B\* in the Coulomb excitation of <sup>8</sup>B on <sup>58</sup>Ni at the beam energy of 25.8 MeV. The dashed and dashed-dotted lines show the cross sections for pure Coulomb and pure nuclear excitation respectively, while the solid line represents their coherent sum.
- Fig. 2 Dipole (solid lines) and quadrupole (dashed lines) components of the angular distributions of the <sup>7</sup>Be fragment emitted in the breakup reaction of <sup>8</sup>B on <sup>58</sup>Ni target at the beam energy of 25.8 MeV. (a) pure Coulomb breakup; also shown here are the *E*1 (solid lines with solid circles) and *E*2 (dashed lines with solid circles) cross sections obtained with point-like projectile and target approximation (Alder-Winther theory), (b) pure nuclear breakup and (c) Coulomb plus nuclear breakup where the corresponding amplitudes are coherently summed.
- Fig. 3 Angular distribution for <sup>8</sup>B+<sup>208</sup>Pb → <sup>8</sup>B\*(<sup>7</sup>Be+p)+ <sup>208</sup>Pb reaction at the beam energy of 415 MeV. (a) Results for pure Coulomb excitation, the dashed and dotted curves represent the E1 and E2 cross sections while their sum is depicted by the solid line. Also shown here are the results obtained with a point-like projectile and target approximation (Alder-Winther theory), where dashed and dotted lines with solid circles show the corresponding E1 and E2 cross sections while the solid line with solid circles represents their sum. (b) Coherent sum of Coulomb and Nuclear excitation calculations; the dashed and dotted lines show the dipole and quadrupole components while the solid line is their sum.
- Fig. 4 Comparison of experimental and theoretical cross section  $\epsilon d\sigma/d\theta$  as a function of the scattering angle  $\theta_{8_{B^*}}$  for  $^8\mathrm{B}+^{208}\mathrm{Pb}\to ^8\mathrm{B}^*(^7\mathrm{Be+p})+^{208}\mathrm{Pb}$  reaction at the beam energy of 415 MeV. Results for three relative energy bins of (a) 500-750 keV, (b) 1250-1500 keV, (c) 2000-2250 keV are shown.  $\epsilon$  is the detector efficiency. Solid lines show the calculated total Coulomb plus nuclear dissociation cross sections while the dashed lines represents the corresponding pure Coulomb dissociation result. Pure quadrupole Coulomb and Coulomb+nuclear cross sections are shown by dotted and dashed-dotted lines. The experimental data and the detector efficiencies are taken from [10].

## **FIGURES**

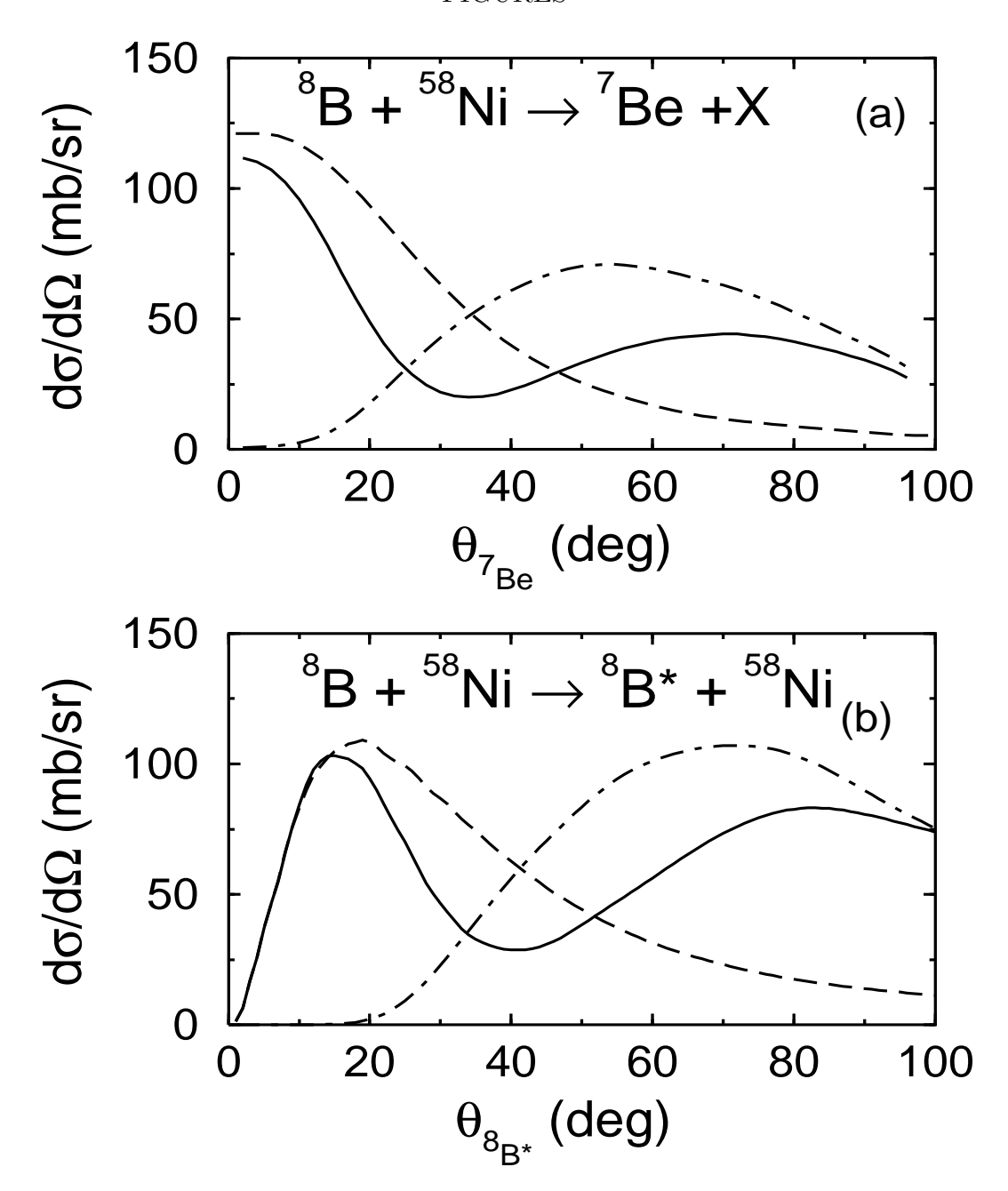


FIG. 1. (a) Angular distribution of the <sup>7</sup>Be fragment emitted in the breakup reaction of <sup>8</sup>B on <sup>58</sup>Ni target at the beam energy of 25.8 MeV. The dashed and dashed-dotted lines show the pure Coulomb and pure nuclear breakup cross sections respectively while their coherent some is represented by the solid line. (b) Angular distribution of <sup>8</sup>B\* in the Coulomb excitation of <sup>8</sup>B on <sup>58</sup>Ni at the beam energy of 25.8 MeV. The dashed and dashed-dotted lines show the cross sections for pure Coulomb and pure nuclear excitation respectively, while the solid line represents their coherent sum.

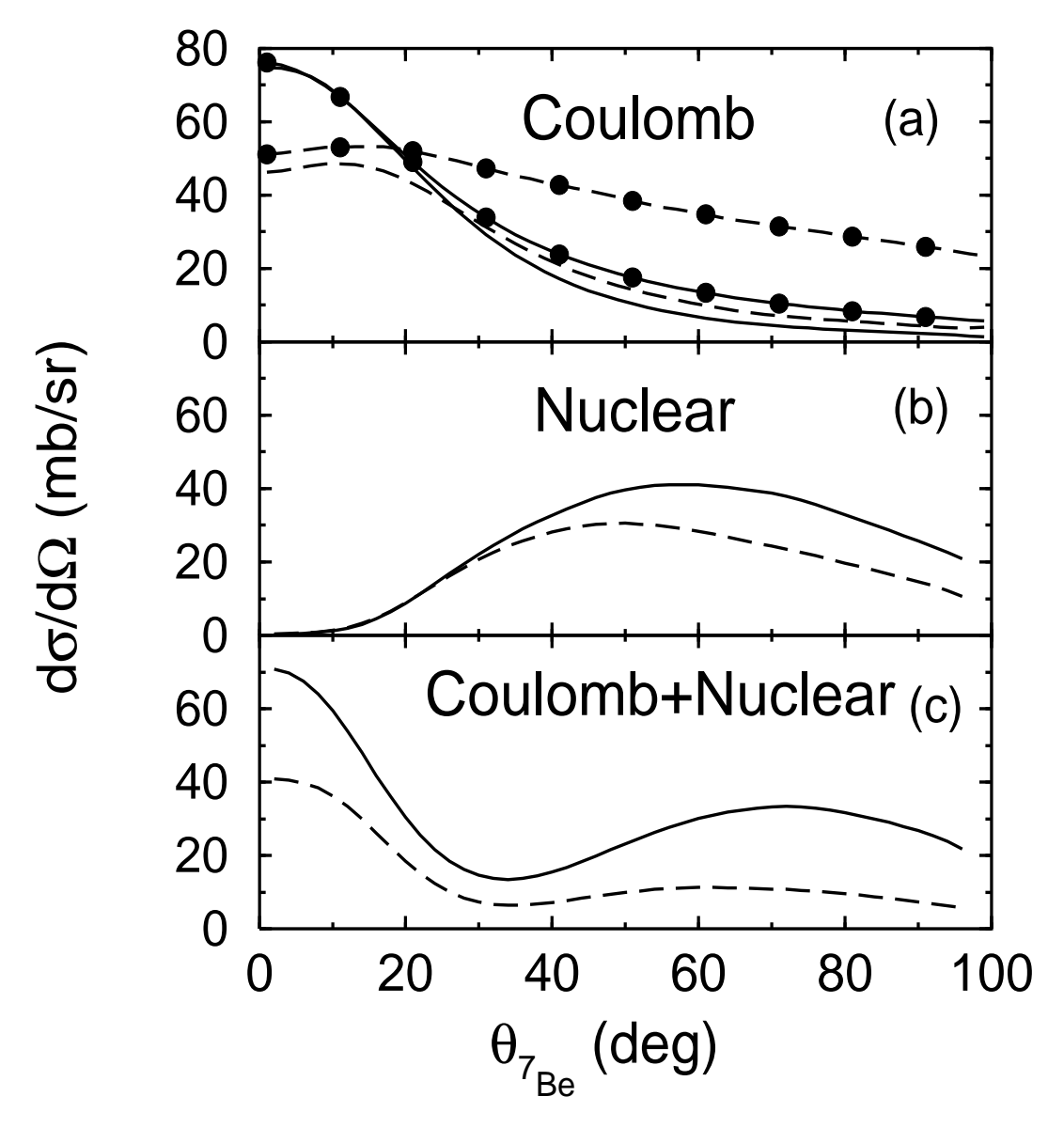


FIG. 2. Dipole (solid lines) and quadrupole (dashed lines) components of the angular distributions of the  $^{7}$ Be fragment emitted in the breakup reaction of  $^{8}$ B on  $^{58}$ Ni target at the beam energy of 25.8 MeV. (a) pure Coulomb breakup; also shown here are the E1 (solid lines with solid circles) and E2 (dashed lines with solid circles) cross sections obtained with point-like projectile and target approximation (Alder-Winther theory), (b) pure nuclear breakup and (c) Coulomb plus nuclear breakup where the corresponding amplitudes are coherently summed.

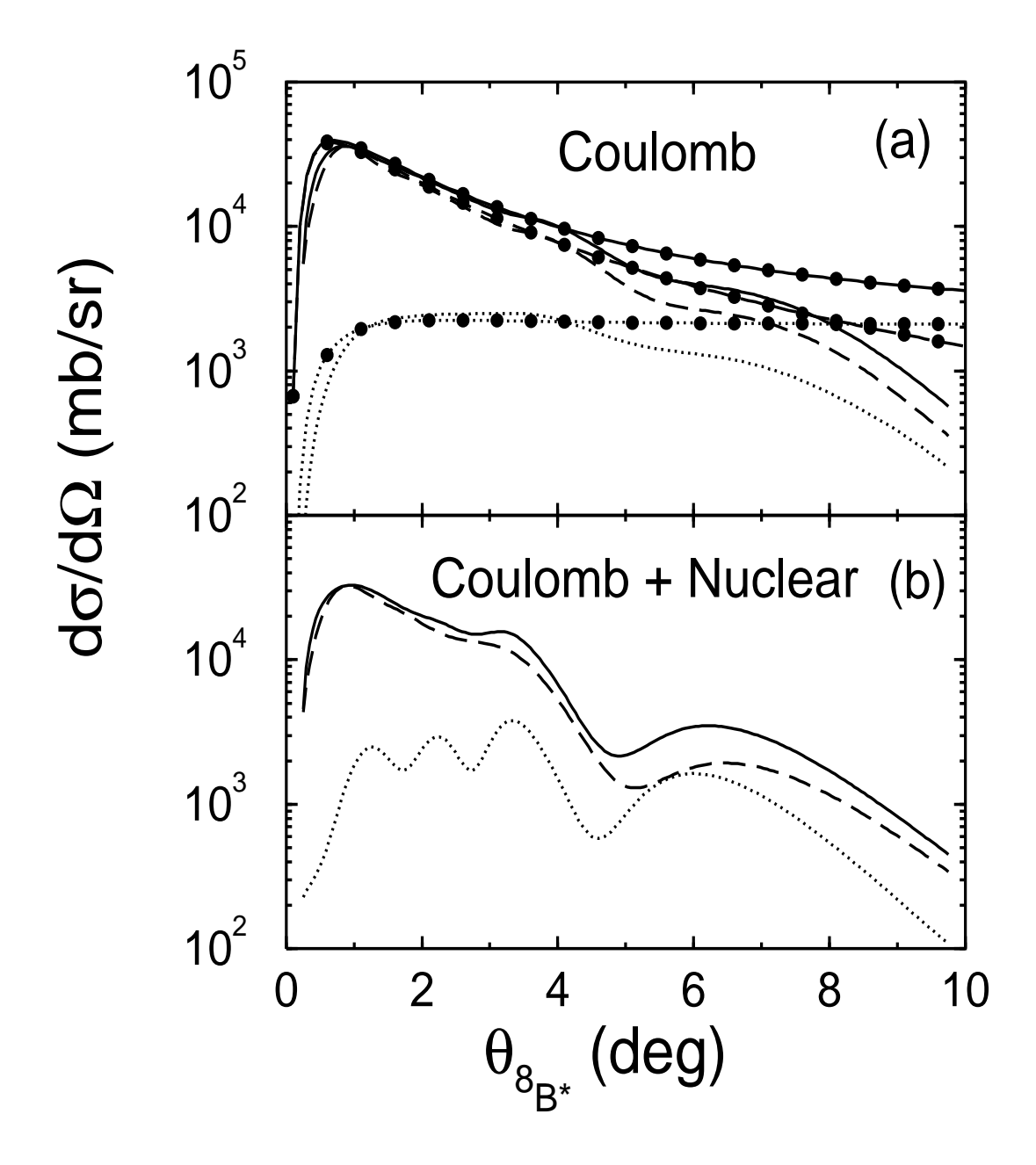


FIG. 3. Angular distribution for  ${}^8B+{}^{208}Pb \rightarrow {}^8B^*({}^7Be+p)+{}^{208}Pb$  reaction at the beam energy of 415 MeV. (a) Results for pure Coulomb excitation, the dashed and dotted curves represent the E1 and E2 cross sections while their sum is depicted by the solid line. Also shown here are the results obtained with a point-like projectile and target approximation (Alder-Winther theory), where dashed and dotted lines with solid circles show the corresponding E1 and E2 cross sections while the solid line with solid circles represents their sum. (b) Coherent sum of Coulomb and Nuclear excitation calculations; the dashed and dotted lines show the dipole and quadrupole components while the solid line is their sum.

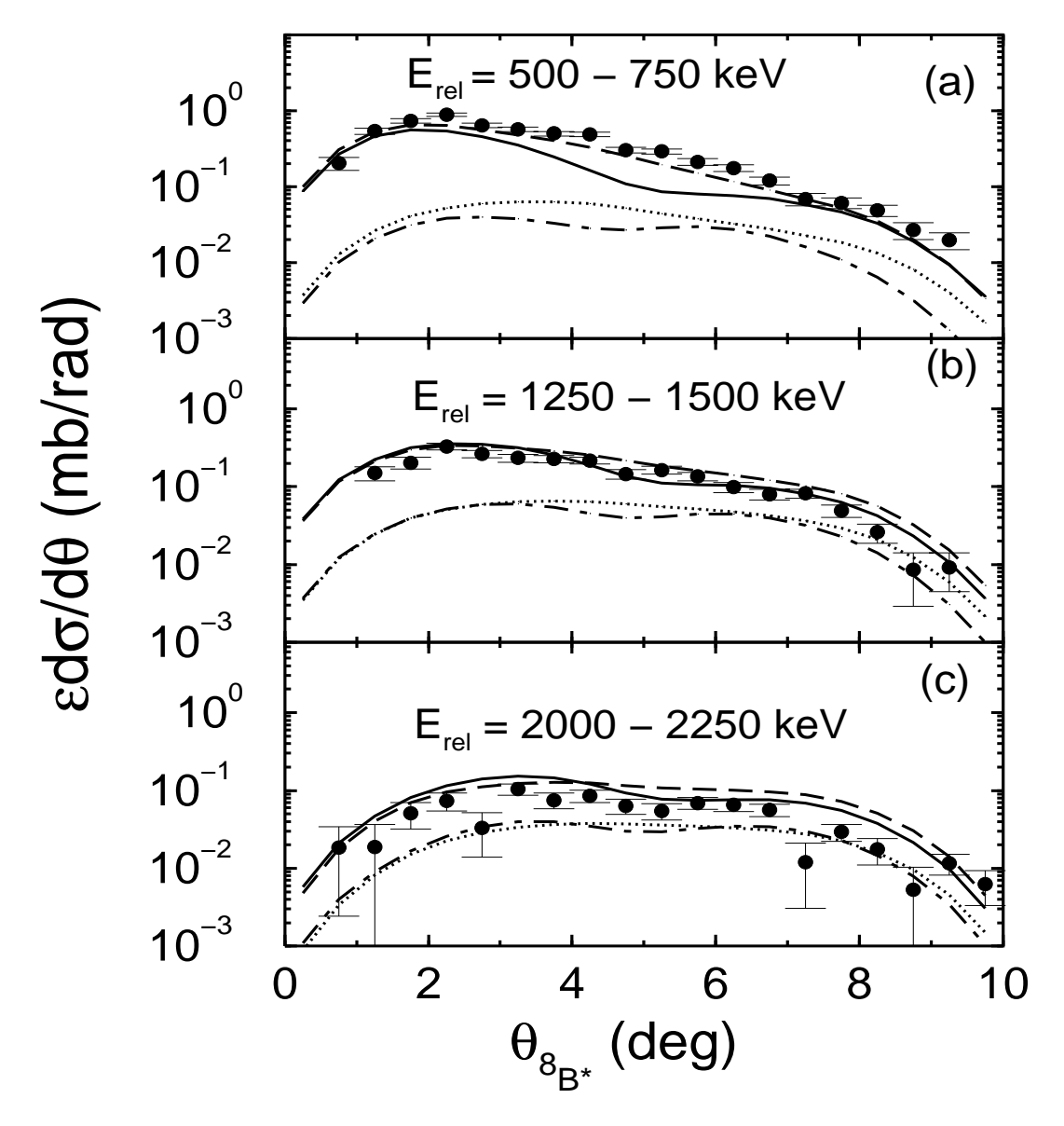


FIG. 4. Comparison of experimental and theoretical cross section  $\epsilon d\sigma/d\theta$  as a function of the scattering angle  $\theta_{8_{B^*}}$  for  $^8\mathrm{B}+^{208}\mathrm{Pb}\to ^8\mathrm{B}^*(^7\mathrm{Be+p})+^{208}\mathrm{Pb}$  reaction at the beam energy of 415 MeV. Results for three relative energy bins of (a) 500-750 keV, (b) 1250-1500 keV, (c) 2000-2250 keV are shown.  $\epsilon$  is the detector efficiency. Solid lines show the calculated total Coulomb plus nuclear dissociation cross sections while the dashed lines represents the corresponding pure Coulomb dissociation result. Pure quadrupole Coulomb and Coulomb+nuclear cross sections are shown by dotted and dashed-dotted lines. The experimental data and the detector efficiencies are taken from [10].